Supplementary Information for

S-scheme Heterojunction of Flake-like $ZnIn_2S_4/SrTiO_3$ Nanosheets for Improved Photocatalytic Performance

Xinyu Yin[a,b], Limin Yu,*[b] Lijing Wang [b], Junjie Zhang[b], Yongya Zhang[b], Fei Li[a], Zhang Fenghua *[a], Wei Wei*[b]

[a] *Liaoning Provincial Key Laboratory of Novel Micro-Nano Functional Materials, School of Petrochemical Engineering, Liaoning Petrochemical University, FuShun 113001, P.R. China*

[b] *College of Chemistry and Chemical Engineering, Shangqiu Normal University, Shangqiu, 476000, P.R. China*

E-mail address: yulimin1234@126.com; zhangfenghua@lnpu.edu.cn; weiweizzuli@163.com

Table of Contents

Section I. Materials and Instrumentation

1.1 Chemicals and Materials

Strontium chloride hexahydrate ($SrCl_2 \cdot 6H_2O$, 99.99%), bismuth oxide (Bi_2O_3, 99.0%), sodium hydroxide (NaOH, ≥ 96.0%), potassium chloride (KCl, 99.8%), indium(III) chloride tetrahydrate ($InCl_3 \cdot 4H_2O$, 99.99%), and thioacetamide (C_2H_5NS, ≥ 99.0%) were all purchased from Shanghai Aladdin Biochemical Technology Co., Ltd. Zinc acetate dihydrate ($C_4H_6O_4Zn \cdot 2H_2O$, 98%) was obtained from Shanghai Macklin Biochemical Technology Co., Ltd. Nano-titanium dioxide (TiO_2, 99.0%) was purchased from Jiangsu Xianfeng Nano Materials Technology Co., Ltd. Sodium oleate ($C_{18}H_{33}NaO_2$, ≥ 98%) was acquired from Shanghai Haohong Biomedical Technology Co., Ltd. Sodium chloride (NaCl, 99%) was purchased from Shanghai Shaoyuan Reagent Co., Ltd.

1.2 Instrumentation

The crystal phase structures of the as-prepared STO, ZIS, and ZIS/STO photocatalysts were characterized via X-ray diffraction using a Shimadzu XRD-6000 diffractometer (Japan) with Cu Kα radiation, over a 2θ range of 10–80°. Scanning electron microscopy images were acquired from a Sigma300 field emission SEM (Zeiss Sigma300, Germany), while transmission electron microscopy images were acquired with an IEOL-JEM-F200 microscope (Japan). X-ray photoelectron spectroscopy was measured on a Thermo Fisher-K-Alpha (USA) X-ray photoelectron spectrometer, and the binding energy was calibrated to 284.8 eV C 1s. Photoluminescence spectra are given by Hitachi F-7100FL the fluorescence spectrometer was detected, and the excitation wavelength was set at 260 nm. The specific surface area was measured by High Performance Microanalyzer (3H-2000PM). Using a UV-visible spectrophotometer (Hitachi U-3900, Japan) the concentration of the TC was determined. Fourier transform infrared spectroscopy analysis was conducted on a Prestige-21 FT-IR spectrometer. The electrochemical properties of STO, ZIS, and ZIS/STO were evaluated using a GHI760E electrochemical workstation (China) with a three-electrode system. Electron spin resonance spectroscopy was performed on an ESR spectrometer at room temperature. The intermediates of LC degradation were detected by liquid chromatography-mass spectrometry.

Section II. Synthetic

2.1 Synthesis of ZIS powder

70 mL of deionized water and 10 mL of glycerol were mixed in a beaker, and the pH of the mixture was adjusted to 3 using 0.5 mol/L hydrochloric acid solution. Subsequently, 0.4307 g of zinc acetate dihydrate of $C_4H_6O_4Zn{\cdot}2H_2O$, 0.4002 g of indium chloride tetrahydrate ($InCl_3{\cdot}4H_2O$), and 0.3004 g of thioacetamide (TAA) were added to the above solution, followed by magnetic stirring for 1 hour. The homogeneous mixture was then transferred into a 200 mL round-bottomed flask. The flask containing the mixed solution was heated with magnetic stirring in an 85 ^oC oil bath for 4. After completion of the oil bath reaction, the mixture was naturally cooled to room temperature, and then washed repeatedly with deionized water and ethanol. Finally, the product was collected by centrifugation and dried to obtain a pale yellowish-white ZIS precipitate.

2.2 Synthesis of STO powder

STO nanosheets were synthesized via a hydrothermal method using $Bi_4Ti_3O_{12}$ as the template and Ti source. $Bi_4Ti_3O_{12}$ was obtained by molten salt method in this study.[1] First, 3.625 g of NaCl and 4.625 g of KCl were ground as cosolvents for 10 min. Stoichiometric amounts of Bi_2O_3 and TiO_2 nanopowders were added at a molar ratio of $NaCl:KCl:Bi_2O_3:TiO_2 = 62.5:62.5:5:7.5$, followed by thorough grinding for 1.5 h. The mixture was transferred into a corundum crucible and calcined at 810 ^oC for 2 h with a heating rate of 5 ^oC /min. After natural cooling, the product was washed with deionized water and ethanol, then dried at 60 ^oC overnight to obtain white $Bi_4Ti_3O_{12}$ powder. The as-prepared $Bi_4Ti_3O_{12}$ was subsequently transformed into STO nanosheets through a topotactic ion-exchange reaction under hydrothermal conditions. In a typical procedure, 0.045 g of sodium oleate (NaOL) was dissolved in 60 mL of 12 mol/L NaOH aqueous solution and stirred for 30 min. Then, 0.8987 g of $SrCl_2{\cdot}6H_2O$ and 0.1498 g of $Bi_4Ti_3O_{12}$ were added, and the mixture was stirred for another 1.5 h. The dispersion was transferred into a 100 mL Teflon-lined autoclave and heated at 220 ^oC for 20 h. During this process, In the strongly alkaline medium (12 M NaOH), Bi^{3+} ions are selectively dissolved from the $Bi_4Ti_3O_{12}$ lattice, while Sr^{2+} ions from $SrCl_2{\cdot}6H_2O$ incorporate into the vacant sites, preserving the layered morphology. Concurrently, the TiO_6 octahedral framework of the precursor remains largely intact, leading to the formation of phase-pure $SrTiO_3$ nanosheets. After hydrothermal treatment, the precipitate was washed with 2 mol/L HNO_3 and ethanol, and dried at 60 ^oC to obtain flake-like STO nanosheets.

2.3 Synthesis of ZIS/STO composite materials

The ZIS/STO composite was fabricated via an in-situ oil bath method. Typically, 0.0143 g of STO nanosheets was dispersed in a mixed solvent of 70 mL deionized water and 10 mL glycerol, followed by sonication for 1 h. The pH of the solution was adjusted to 3 using 0.5 mol/L HCl. Then, 0.4307 g of $C_4H_6O_4Zn{\cdot}2H_2O$, 0.4002 g of $InCl_3{\cdot}4H_2O$, and 0.3004 g of TAA were added and stirred until fully dissolved. The mixture was transferred into a 200 mL round-bottom flask and heated in an oil bath at 85 ^oC with magnetic stirring for 4 h. After cooling to room temperature, the product was washed with deionized water and ethanol, collected by centrifugation, and dried at 60 ^oC to obtain a yellow ZIS/STO composite. The resulting composite exhibited a ZIS to STO mass ratio of approximately 1:2, which was identified as the optimal ratio through preliminary screening experiments. The adjustment of solution pH to 3 prior to deposition serves primarily to protonate the substrate surface , rendering it positively charged,[2] thereby facilitating the adsorption of negatively charged metal precursor complexes via electrostatic interactions.[3] This approach has been widely employed to regulate the growth and interfacial bonding of $ZnIn_2S_4$ materials,[4, 5] contributing to the formation of dense and robust heterojunction thin films.

2.4 Photocatalytic hydrogen evolution.

The photocatalytic hydrogen production performance was evaluated in a closed photoreaction system. First, 30 mg of the catalyst was dispersed in 50 mL of 10 vol.% triethanolamine (TEOA) aqueous solution and sonicated to achieve uniform dispersion. Subsequently, the resulting suspension was transferred into a quartz photoreactor, which was then evacuated to remove air. The reaction was conducted under irradiation from a 300 W xenon lamp with a light power density of 100 mW cm^{-2}, positioned 15 cm away from the reaction solution. The temperature was maintained stable by a circulating water cooling system. The produced hydrogen was quantitatively analyzed using a gas chromatograph (GC), and the H_2 production rate was calculated based on the fitted standard calibration curve. In addition, five consecutive cyclic tests were performed, with each cycle lasting 5 h and the H_2 production measured each hour. After each cycle, the photocatalyst was recovered by centrifugation, washed to remove adsorbed residual sacrificial agent and oxidation products, and then reused for the subsequent photocatalytic test. The apparent quantum efficiency (AQE) of the ZIS/STO photocatalyst was evaluated using a procedure similar to that of the photocatalytic H_2 evolution experiments, where monochromatic light was generated using band-pass filters at 400, 405, 435, and 475 nm. The apparent quantum efficiency (AQE) was calculated by the Equation 1:[6]

$$\mathrm{AQE}(\%) = \frac{2 \times \text{number of evolved } H_2 \text{ molecules}}{\text{number of incident photons}} \times 100\% = \frac{2nN_A hc}{PS\lambda t} \times 100\%$$

where n is the evolution amount of H_2, N_A is Avogadro's constant, h is Planck's constant, c is the speed of light, λ is the wavelength of the incident light, P is the power density, S is the light exposure area, and t is the reaction time.

2.5 Photocatalytic degradation

In this experiment, a 300 W xenon arc lamp was used to simulate sunlight, with a light power density of 40.0 mW/cm^2. 10 mg of the photocatalyst was dispersed in 50 mL of TC solution (10 mg/L), followed by stirring in the dark for 30 min to perform the dark reaction, ensuring the achievement of adsorption-desorption equilibrium prior to light irradiation. After light on, 2.5 mL solution was taken every 15 min, the catalyst was filtered out of the solution with a 0.45 μm drainage filter, and the residual concentration of tetracycline was monitored using a UV–vis spectrophotometer. Based on the TC concentration in the filtrate, the photocatalytic efficiency and kinetics of photoinduced degradation were determined via the following equation.

$$\eta\% = C_0/C \times 100\% \quad (1)$$

$$\ln(C_0/C) = kt \quad (2)$$

C_0 and C denote the initial concentration of TC and the concentration of TC at time t, respectively. k represents the apparent rate constant, and t stands for the reaction time. Additionally, cyclic experiments were also conducted. The degradation process was carried out as described above. After each round of photocatalytic degradation experiment, the spent ZIS/STO composite was rinsed repeatedly with deionized water several times and then dried in an oven at 70 °C. Subsequently, the degradation experiment was performed again under the same conditions, and this process was repeated four times.

2.6 Photodegradation Experiments Under Different pH Conditions

In practical applications, numerous factors can affect the degradation efficiency. Therefore, to evaluate the photocatalytic degradation activity of the photocatalyst toward TC, the influence of pH value was investigated. First,

tetracycline solution with a concentration of 10 mg/L was prepared, and then 50 mL of the solution was used to adjust the pH value of 1, 3, 5, 7, 9, 11, 13 and 14 with HCl and NaOH, respectively. Subsequently, 10 mg of the photocatalyst was sequentially dispersed in the TC aqueous solutions with different pH values, followed by stirring in the dark for 30 min to ensure the achievement of adsorption-desorption equilibrium before light irradiation. After light on, 2.5 mL solution were collected at 15-minute intervals, and the catalyst was filtered out from the solution using a 0.45 μm aqueous system filter. The residual concentration of TC was monitored by a UV-Vis spectrophotometer.

2.7 Photodegradation Experiments in the Presence of Different Anions and Cations

Since various anions and cations may exist in aqueous environments and exert a certain impact on photodegradation efficiency, this study aimed to evaluate the tolerance of the constructed photocatalytic system to ionic interference. First, tetracycline solution with a concentration of 10 mg/L was prepared, and then 50 mL aliquots of this solution were taken, and the following salts of 5 mg was added separately: $NaNO_3$, NaCl, Na_2CO_3, Na_2SO_4, KNO_3, $Ca(NO_3)_2$, $Mg(NO_3)_2$, and $Cu(NO_3)_2$. Subsequently, 10 mg of the photocatalyst was dispersed in the 50 mL TC solution containing different anions and cations. The mixture was first stirred in the dark for 30 min to ensure the achievement of adsorption-desorption equilibrium, followed by turning on the xenon lamp for light irradiation. After light on, 2.5 mL solution were collected at 15-minute intervals, and the catalyst was filtered out from the solution using a 0.45 μm aqueous system filter. The residual concentration of TC was monitored by a UV-Vis spectrophotometer.

2.8 Photodegradation Experiments of Different Antibiotics

In actual aqueous environments, multiple pollutants may coexist. To evaluate the versatility of the composite catalyst, photodegradation experiments were conducted on different antibiotics. First, 10 mg/L aqueous solutions of amoxicillin, ceftiofur, rhodamine B, and norfloxacin were prepared. Subsequently, 10 mg of the photocatalyst was sequentially dispersed in each of the different antibiotic solutions, followed by stirring in the dark for 30 min to ensure the achievement of adsorption-desorption equilibrium. After that, the xenon lamp was turned on for light irradiation. After light on, 2.5 mL solution were collected at 15-minute intervals, and the catalyst was filtered out from the solution using a 0.45 μm aqueous system filter. The residual concentration of the corresponding antibiotic was monitored by a UV-Vis spectrophotometer.

2.9 Free radical capture experiment

To identify the active species generated during the reaction, different scavengers were added to the reaction system. Generally, ascorbic acid (VC), ammonium oxalate (AO), and isopropyl alcohol (IPA) were used to scavenge $\cdot O_2^-$, h^+, and $\cdot OH$, respectively. Arrange 50 mg/L of tetracycline solution, then take 50 mL solution and add 10 mg of capture agent. Subsequently, The weighing photocatalyst (30 mg) was dissolved in 50 mL of tetracycline solution containing different scavengers, followed by stirring in the dark for 30 min to ensure adsorption-desorption equilibrium prior to light irradiation. After light on, 2.5 mL solution were collected at 15-minute intervals, and the catalyst was filtered out from the solution using a 0.45 μm aqueous system filter. The residual concentration of TC was monitored by a UV-Vis spectrophotometer.

Section III. Characterization

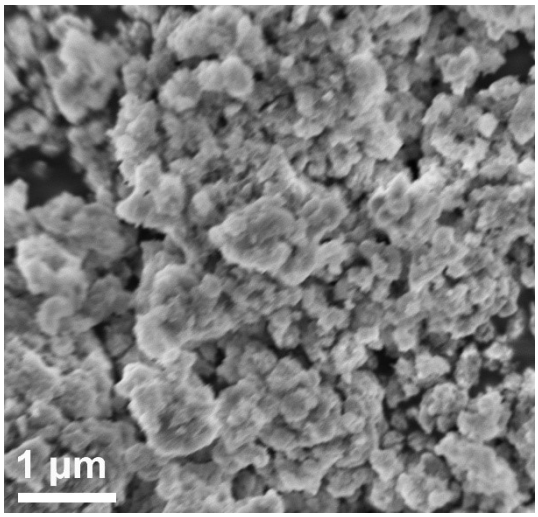

Fig. S1 SEM images of the ZIS nanoparticles.

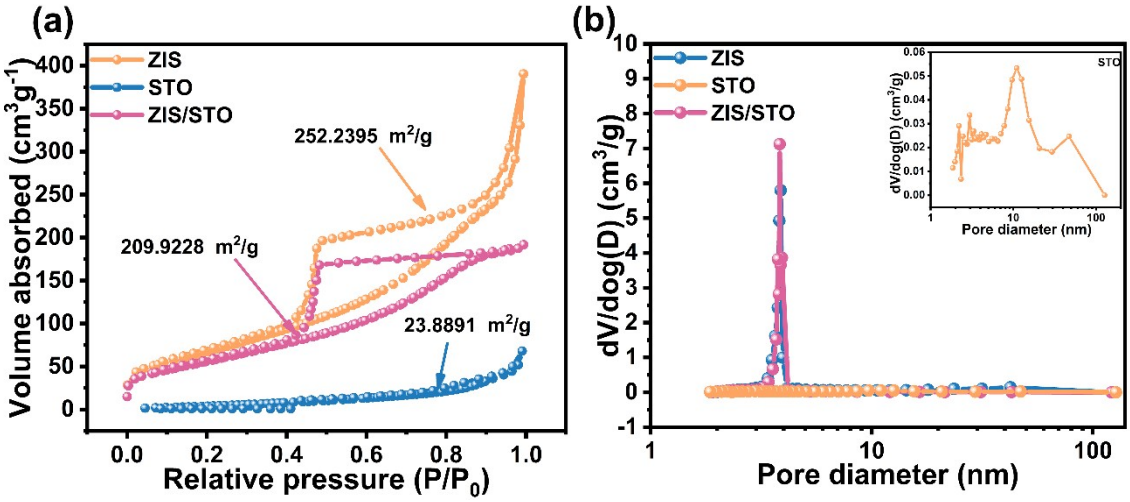

Fig. S2 N_2 adsorption-desorption isotherm and the pore size distribution of pristine ZIS, STO, and the ZIS/STO composite.

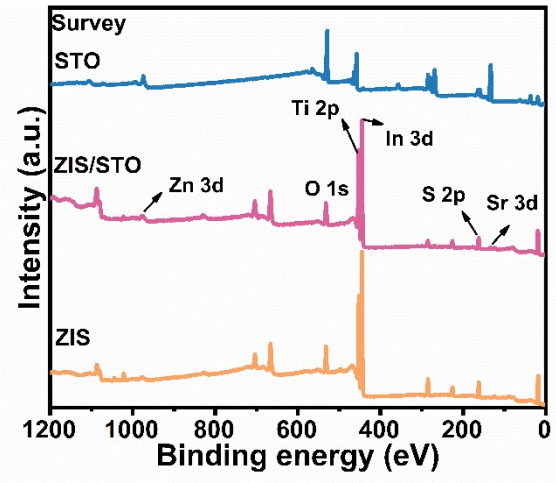

Fig. S3 XPS spectrum of ZIS, STO, and ZIS/STO.

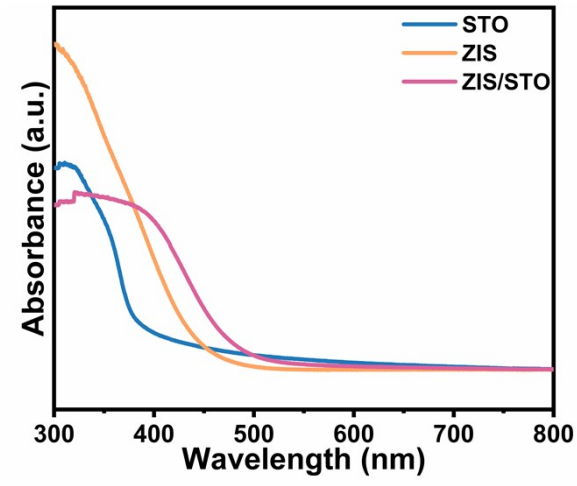

Fig. S4 UV-vis DRS of ZIS, STO and ZIS/STO.

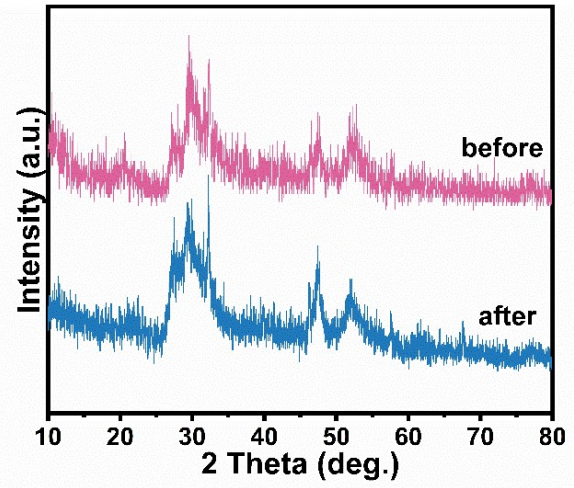

Fig. S5 XRD pattern of ZIS/STO sample after photocatalytic reaction.

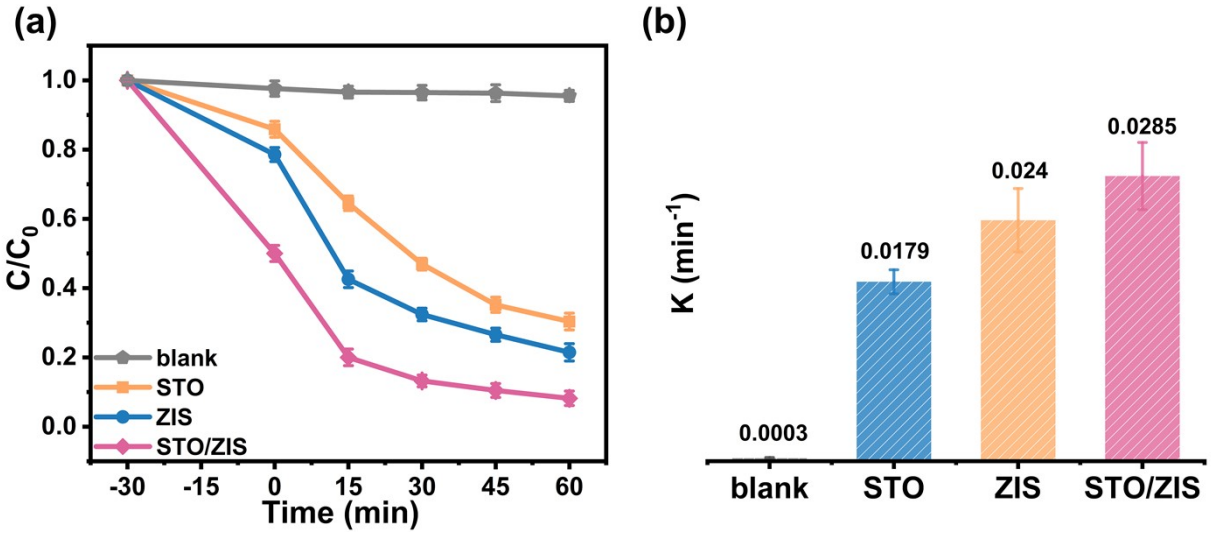

Fig. S6 (a) Photocatalytic TC degradation performance, (b) The removal kinetic rates of different catalysts.

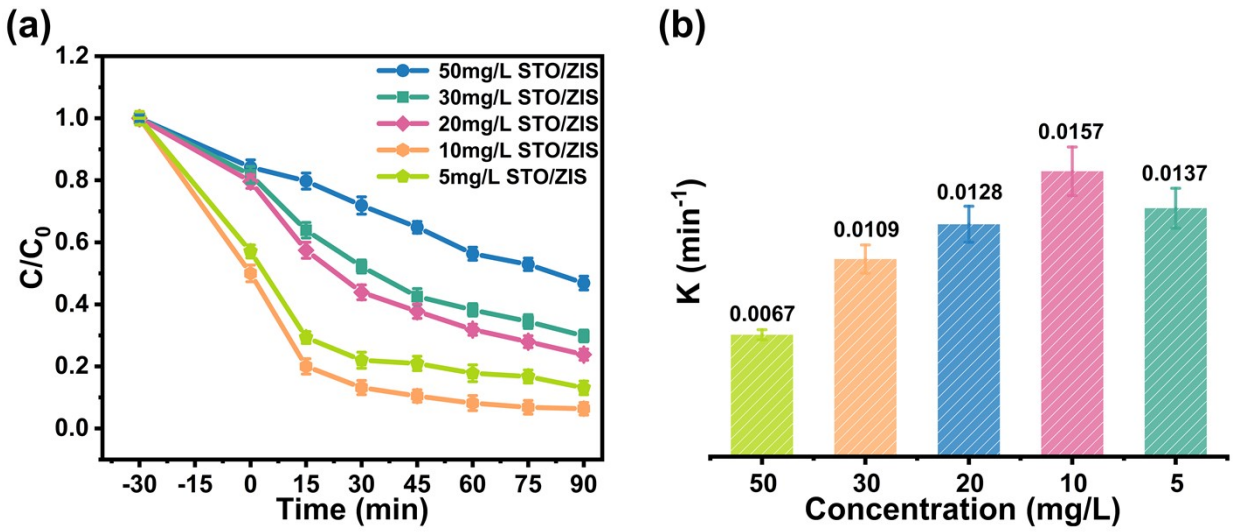

Fig. S7 The effect of (a) tetracycline concentration, (b) The removal kinetic rates for different concentrations of tetracycline.

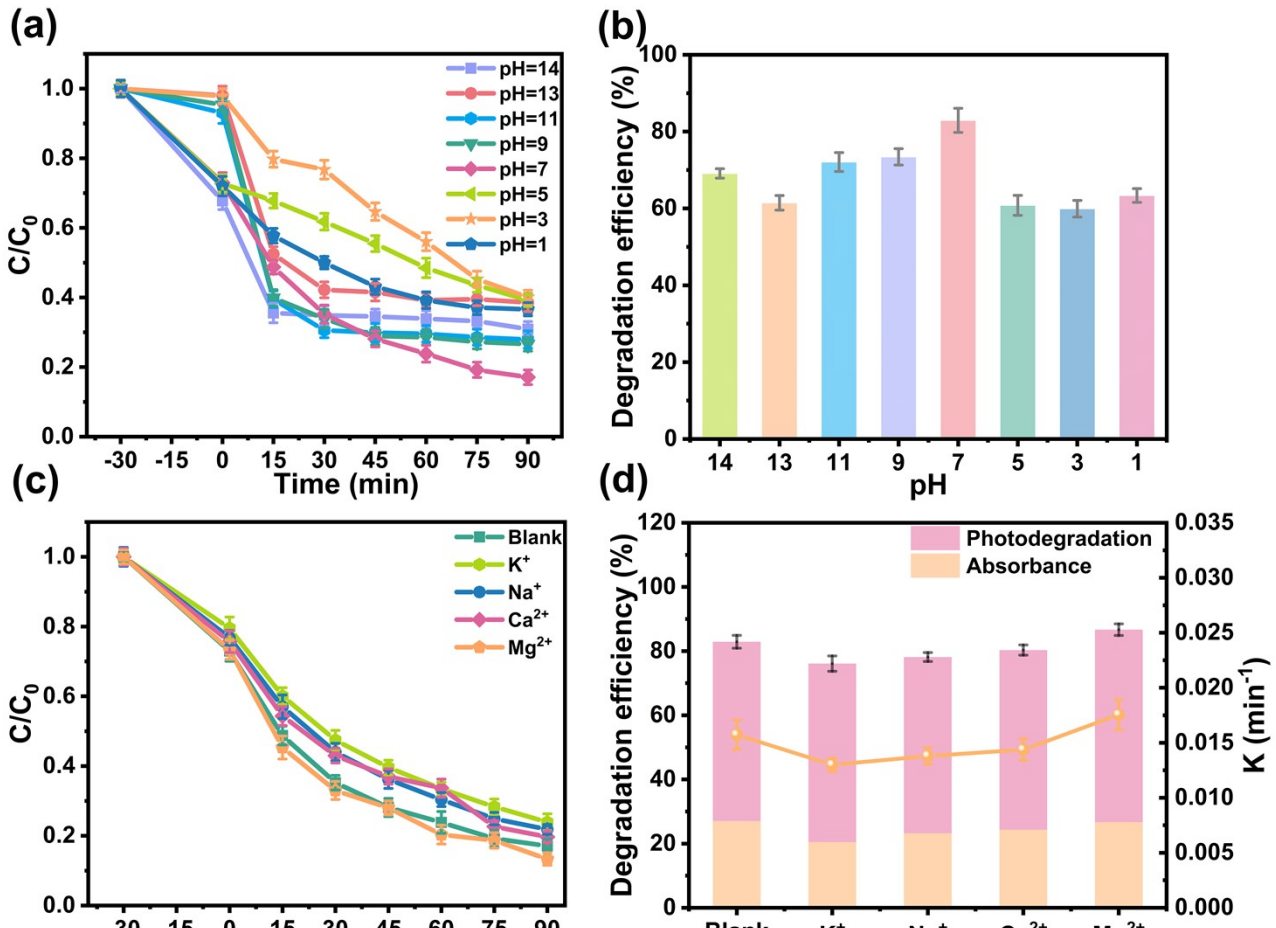

Fig. S8 (a) ZIS/STO photocatalysts at different pH and (b) the degradation rate, (c) ZIS/STO photocatalyst under different cationic conditions and (d) the degradation rate and removal kinetic rates, (e) ZIS/STO photocatalyst under different anionic conditions and (f) the degradation rate and removal kinetic rates.

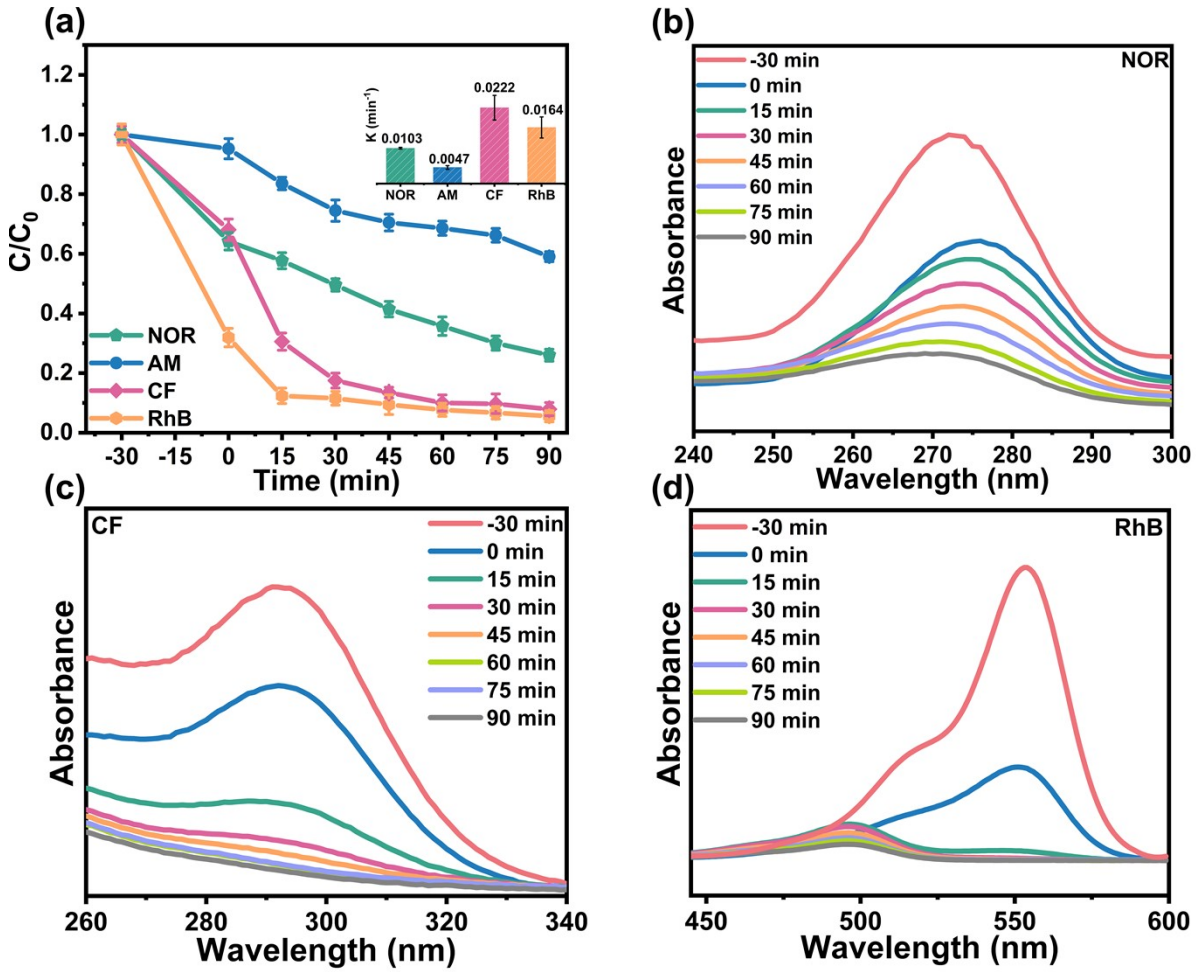

Fig. S9 (a)ZIS/STO photocatalyst under different antibiotic conditions. UV-Vis absorption spectra of different antibiotics, corresponding to (b) CF, (c)RhB, (d) NOR.

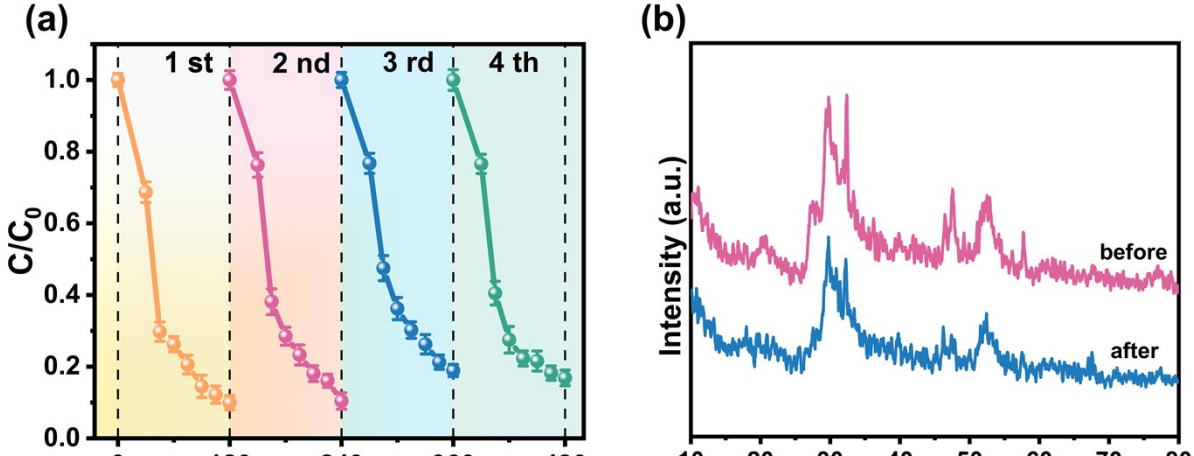

Fig. 10 (a) Cycling process of photocatalytic TC degradation by ZIS/STO, (b) XRD profile of ZIS/STO before and after the photocatalytic degradation reaction.

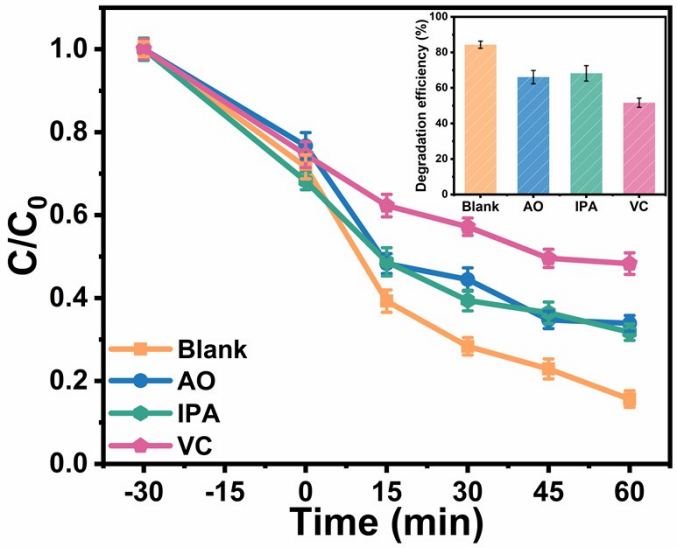

Fig. S11 Effect of different quenchers on the photocatalytic degradation of ZIS/STO under solar light irradiation.

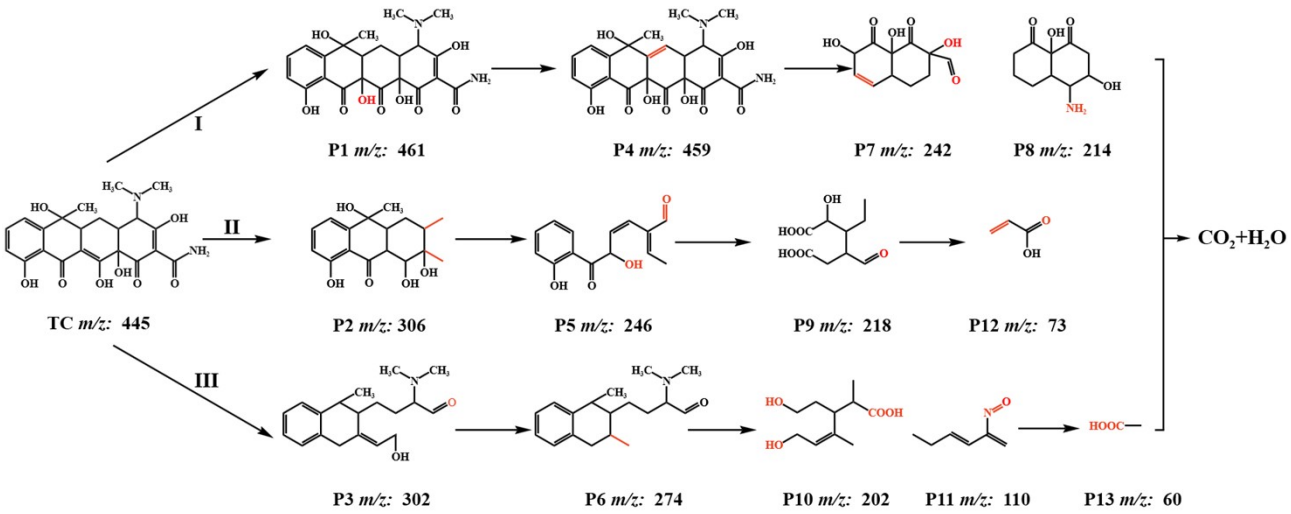

Fig. 12 The degradation mechanism of TC.

Table 1 The comparison of photocatalytic H_2-production activity of ZIS/STO with previous literatures.

Catalyst	**Sacrificial reagents**	**Catalyst loading**	**Rate of H_2 production ($mmol \cdot g^{-1} \cdot h^{-1}$)**	**Light source**	**Reference**
Ti_3C_2-MXene/ $ZnIn_2S_4$	1.0 M TEOA	100 mg / 80 mL	0.9787 $mmol \cdot g^{-1} \cdot h^{-1}$	300 W Xe lamp; $\lambda > 420$ nm	7
Ti_3C_2@TiO_2/$ZnIn_2S_4$	0.35 M Na_2S and 0.25 M Na_2SO_3	15 mg / 80 mL	1.1858 $mmol \cdot g^{-1} \cdot h^{-1}$	300 W Xe lamp	8
$AgIn_5S_8$/$ZnIn_2S_4$	0.25 M Na_2S and 0.25 M Na_2SO_3	50 mg / 100 mL	0.9499 $mmol \cdot g^{-1} \cdot h^{-1}$	300 W Xe lamp; $\lambda > 420$ nm	9
PMo_{12}/ $MgIn_2S_4$	0.2 M $C_3H_6O_3$	20 mg / 50 mL	0.2325 $mmol \cdot g^{-1} \cdot h^{-1}$	300 W Xe lamp; $\lambda > 420$ nm	10
CeO_2/$ZnIn_2S_4$	0.35 M Na_2S and 0.25 M Na_2SO_3	50 mg / 200 mL	0.8474 $mmol \cdot g^{-1} \cdot h^{-1}$	300 W Xe lamp	11
$MgIn_2S_4$@1T/2H-MoS_2	10% methanol solution	20 mg / 20 mL	0.37 $mmol \cdot g^{-1} \cdot h^{-1}$	150 W Xe lamp; $\lambda > 420$ nm	12
In_2O_3/CdZnS	Na_2S/Na_2SO_3	8 mg / 100 mL	1.13 $mmol \cdot g^{-1} \cdot h^{-1}$	300 W Xe lamp	13
CuO-In_2O_3	TEOA	10 mg / 8 mL	0.6 $mmol \cdot g^{-1} \cdot h^{-1}$	300 W Xe lamp	14
$ZnIn_2S_4$/ $SrTiO_3$	**TEOA**	**30 mg /50 mL**	**1.380 $mmol \cdot g^{-1} \cdot h^{-1}$**	**300 W Xe lamp**	**This work**

Table 2. Calculated apparent quantum efficiency (AQE) at different wavelengths

Wavelength	H_2 Evolved (μmol)	Light Intensity	AQE(%)
λ = 400 nm	12.97	20.38 mW	2.12%
λ = 405 nm	9.43	17.67 mW	1.75%
λ = 435 nm	4.37	16.24 mW	0.82%
λ = 475 nm	2.03	15.92 mW	0.36%

λ = 400 nm:

$$\text{Number of incident photons (N)} = \frac{E\lambda}{hc} = \frac{20.38 \times 10^{-3} \times 5 \times 3600 \times 400 \times 10^{-9}}{6.626 \times 10^{-34} \times 3 \times 10^{8}}$$

$$= 7.38 \times 10^{20}$$

$$\text{AQE\%} = \frac{2 \times \text{Number of evolved } H_2 \text{ molecules}}{\text{N}} \times 100\%$$

$$= \frac{2 \times 6.02 \times 10^{23} \times 12.97 \times 10^{-6}}{7.38 \times 10^{20}} \times 100\% = 2.12\%$$

λ = 405 nm:

$$\text{Number of incident photons (N)} = \frac{E\lambda}{hc} = \frac{17.67 \times 10^{-3} \times 5 \times 3600 \times 405 \times 10^{-9}}{6.626 \times 10^{-34} \times 3 \times 10^{8}}$$

$$= 6.48 \times 10^{20}$$

$$\text{AQE\%} = \frac{2 \times \text{Number of evolved } H_2 \text{ molecules}}{\text{N}} \times 100\%$$

$$= \frac{2 \times 6.02 \times 10^{23} \times 9.43 \times 10^{-6}}{6.48 \times 10^{20}} \times 100\% = 1.75\%$$

λ = 435 nm:

$$\text{Number of incident photons (N)} = \frac{E\lambda}{hc} = \frac{16.24 \times 10^{-3} \times 5 \times 3600 \times 435 \times 10^{-9}}{6.626 \times 10^{-34} \times 3 \times 10^{8}}$$

$$= 6.39 \times 10^{20}$$

$$\text{AQE\%} = \frac{2 \times \text{Number of evolved } H_2 \text{ molecules}}{\text{N}} \times 100\%$$

$$= \frac{2 \times 6.02 \times 10^{23} \times 4.37 \times 10^{-6}}{6.39 \times 10^{20}} \times 100\% = 0.82\%$$

λ = 475 nm:

$$\text{Number of incident photons (N)} = \frac{E\lambda}{hc} = \frac{15.92 \times 10^{-3} \times 5 \times 3600 \times 475 \times 10^{-9}}{6.626 \times 10^{-34} \times 3 \times 10^{8}}$$

$$= 6.84 \times 10^{20}$$

$$AQE\% = \frac{2 \times \text{Number of evolved } H_2 \text{ molecules}}{N} \times 100\%$$

$$= \frac{2 \times 6.02 \times 10^{23} \times 2.03 \times 10^{-6}}{6.84 \times 10^{20}} \times 100\% = 0.36\%$$

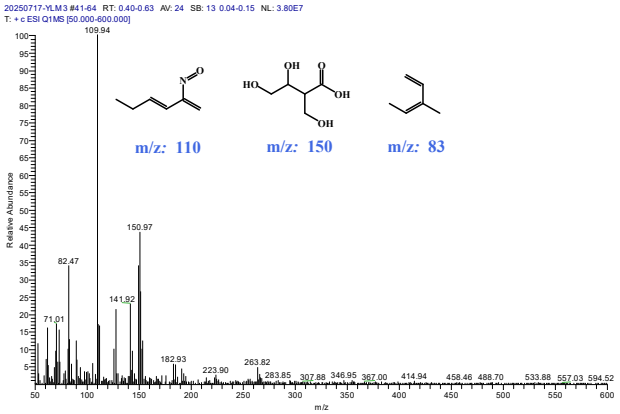

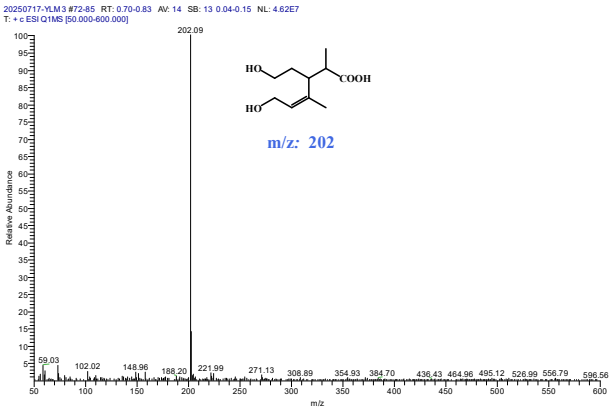

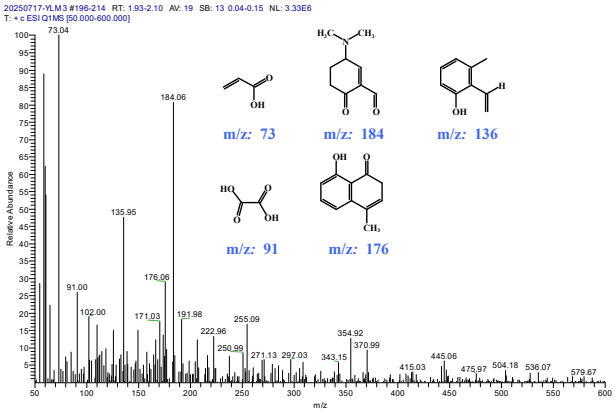

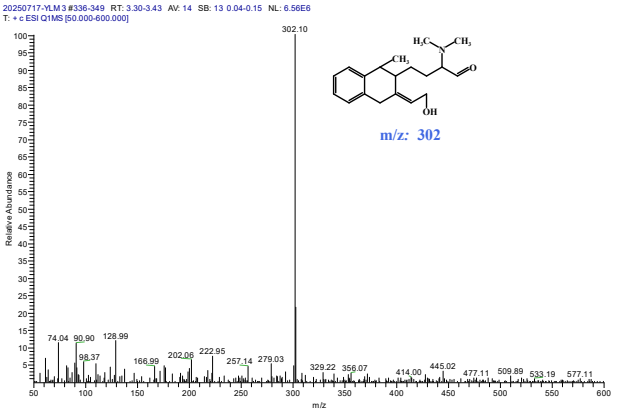

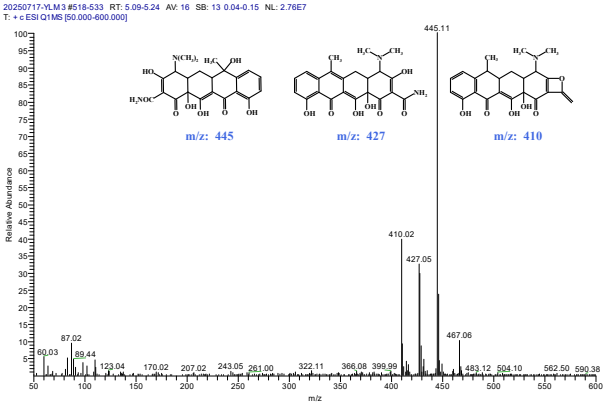

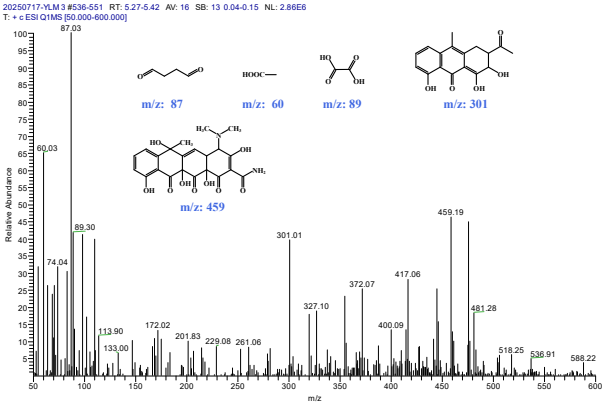

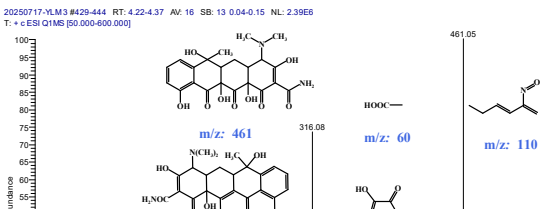

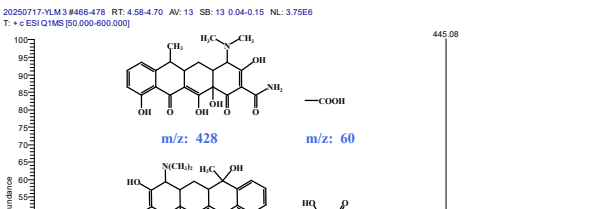

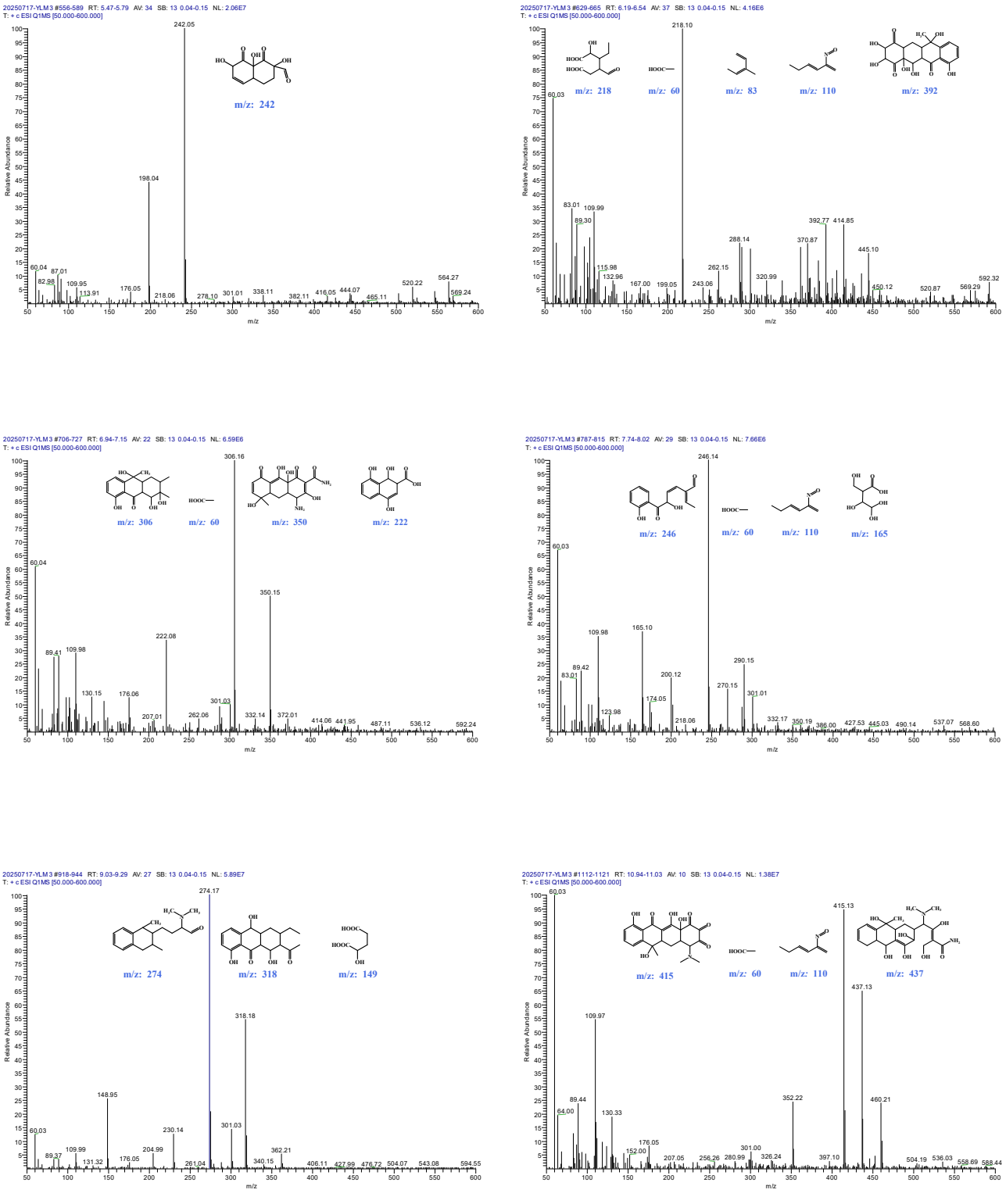

Fig. S13 Mass spectral database for decomposition products of TC.

References

1 Y. Liu, G. Zhu, J. Peng, J. Gao, C. Wang and P. Liu, *J. Mater. Sci. Mater. Electron*., 2017, **28**(2), 2172-2182.

2 M. Kosmulski, *Adv. Colloid Interface Sci*., 2023, **319**, 102973.

3 Y. Ma, A. N. Kuhn, W. Gao, T. Al-Zoubi, H. Du, X. Pan and H. Yang, *Nano Energy.*, 2021, **79**, 105465.

4 Q. Xi, F. Xie, J. Liu, X. Zhang, J. Wang, Y. Wang, Y. Wang, H. Li, Z. Yu, Z. Sun, X. Jian, X. Gao, J. Ren, C. Fan and R. Li, *Small.*, 2023, **19**, 2300717.

5 R. Bariki, K. Das, S. K. Pradhan, B. Prusti and B. G. Mishra, *ACS Appl. Energy Mater*., 2022, **5**, 11002-11017.

6 X. Wang, X. Wang, H. Yang, A. Meng, Z. Li, L. Yang, L. Wang, S. Li, G. Li and J. Huang, *Chem. Eng. J.*, 2022, **431**, 134000.

7 W. Huang, Z. Li, C. Wu, H. Zhang, J. Sun, Q. Li, *J. Mater. Sci. Technol*., 2022, **120**, 89-98.

8 K. Huang, C. Li and X. Meng, *J. Colloid Interface Sci*., 2020, **580**, 669-680.

9 Z. Guan, Z. Xu, Q. Li, P. Wang, G. Li and J. Yang, *Appl Catal B*., 2018, **227**, 512-518.

10 A. Rong, H.F. Shi, Q. Zhao, H.W. Zhu, H.S. Wang, G. Yan, *Sep. Purif. Technol*., 2024, **348**, 127782.

11 M. Zhang, J. Yao, M. Arif, B. Qiu, H. Yin, X. Liu and S.-m. Chen, *Appl. Surf. Sci.*, 2020, **526**, 145749.

12 S. Das, L. Acharya, L. Biswal, K. Parida, *Nanoscale Adv*., 2024, **6**, 934.

13 H. Yang, J. Tang, Y. Luo, X. Zhan, Z. Liang, L. Jiang, H. Hou, W. Yang, *Small.*, 2021, **17**, 2102307.

14 L. Sun, Y. Zhuang, Y. Yuan, W. Zhan, X.J. Wang, X. Han, Y. Zhao, *Adv. Energy Mater*., 2019, **9**.